Comparison of MPS and SPH methods for solving forced motion ship flooding problems

Hirotada Hashimoto, Nicolas Grenier, Makoto Sueyoshi, David Le Touzé

Version of Record: https://www.sciencedirect.com/science/article/pii/S0141118721004636
Manuscript_662dd11b80154c5bf817894089d1f750

Comparison of MPS and SPH methods for solving forced motion ship flooding problems

Hirotada Hashimoto[1], Nicolas Grenier[2], Makoto Sueyoshi[3], David Le Touzé[4],

1. Graduate School of Engineering, Osaka Prefecture University, Sakai, Osaka, Japan
2. Université Paris-Saclay, CNRS, LISN, Orsay, France
3. Research Institute for Applied Mechanics, Kyushu University, Kasuga, Fukuoka, Japan
4. Ecole Centrale Nantes, LHEEA Lab. (ECN / CNRS), Nantes, France

Corresponding author: Nicolas Grenier, nicolas.grenier@lisn.upsaclay.fr

ABSTRACT:

In order to assess the safety of damaged ships quantitatively, advanced numerical simulation methods are required for the prediction of ship dynamic behavior coupled with floodwater. For the prediction of fast and complicated free-surface flows in immediate flooding, particle methods are promising because largely deformed free-surface can be naturally and accurately followed without numerical diffusion. In this paper, systematic comparisons of the MPS (Moving Particle Semi-implicit) and SPH (Smoothed Particle Hydrodynamics) methods are made on ship flooding problems. Firstly, numerical simulations based on the MPS and SPH methods are performed on forced roll tests of a two-dimensional damaged compartment and are compared with a dedicated model experiment. Secondly, similar comparisons are made for a three-dimensional flooded compartment. Through these comparisons between MPS and SPH methods and to model-scale experiments, the capability of particle methods in simulating complicated flooding flows is investigated and the difference of prediction accuracy of the MPS and SPH methods is discussed. For the case of two-dimensional damaged compartment, it is also studied what effects has a single-phase approximation in comparison to simulations where air is modelled, and how the trapped air in damaged compartments influences the water flow evolution. Results from this study show that both particle methods are capable to simulate complex flooding flows in good quantitative agreement with respect to experiments and with similar execution times while there is no possibility to draw superiority of one method. However when dealing with air modelling, using a simplified approach limits computational times but induces quite large discrepancies compared to fully modelling the air phase.

Keywords: Particle methods; MPS; SPH; Ship flooding; Forced roll test; Trapped air

1. INTRODUCTION

Collision and grounding accidents of ships are frequently reported even nowadays while human and environmental security issues are carefully looked by societies. Securing the survivability against flooding is one of the most important requirements in ship design [1]. Since the quantitative prediction of ship transient behavior induced by the floodwater inflow is essential to ensure the safety of damaged ships, advanced numerical simulation methods are strongly desired especially for immediate flooding leading to capsizing. These methods must be able to accurately predict the strongly nonlinear free-surface flow occurring into damaged compartments through damage openings and progressive flooding into all floodable compartments. In addition, the dynamic coupling between floodwater and ship motion must also be considered. Therefore, the development of advanced numerical methods in time domain, which enable to simulate dynamic motions of damaged ships from the initial stage of water flooding to the final equilibrium or catastrophic state, is crucial to fully account for the complexity of these floodwater flows.

This problem can be studied either experimentally (see, e.g., [2, 3]) or using conventional mesh-based CFD (Computational Fluid Dynamics) methods (see, e.g., [4, 5, 6]) while progressive flooding is still often studied with linearized algebraic formulations [7]. For solving violent flows of flooding, e.g. abrupt flooding through damaged openings or progressive flooding with sloshing and up- and down-flooding, particle methods, thanks to their Lagrangian formalism which naturally includes nonlinear transport term and preserves sharp interfaces, present interesting features to describe nonlinear free-surface flows. Beyond providing an accurate and perfectly non-diffusive description of complex fluid interfaces, the Lagrangian nature of particle methods permits to avoid the discretization of the convection term of Navier-Stokes equations, thus providing a source of accuracy when flows are dominated by inertia, as are violent flows (no numerical diffusion on this term). The two main particle methods to simulate complex free-surface flows are the SPH (Smoothed Particle Hydrodynamics) and MPS (Moving Particle Semi-implicit) methods, which are closely related. Regarding complex flooding flow problems, several studies can be found with these methods. González et al. [8] simulated the shallow water flow in flooded car deck by SPH. Skaar et al. [9] predicted progressive flooding of a complicated two-dimensional ship section by SPH. Le Touzé et al. [10] and Oger et al. [11] simulated flooding in ship internal compartments by SPH. Zhang et al. [12] and Guo et al. [13] predicted sinking of a simple 3-D damaged model by SPH. Later, Ming et al. [14] predicted sinking of a similar compartment in beam waves. Cao et al. [15] included the influence of air on a two-dimensional damaged cabin simulated by a multiphase SPH method. Hashimoto et al. [16,17] predicted transient and dynamic behaviors of a damaged PCTC (Pure Car and Truck Carrier) in flooding situations, with a hybrid scheme using ordinary potential theory for intact hull and the MPS method for damaged hull. The numerical technique, solving an equation of ship motion and the Navier-Stokes equation by the MPS method simultaneously in the framework of weakly nonlinear analysis, is useful for ship motions

coupled with fluid flows [18,19]. Zhang et al. [20] studied flooding of different ship sections with the MPS method and analyzed impact of damage position on ship motion and flooding.

Although the existing works mentioned above well demonstrated that particle methods are promising approaches for the safety assessment of damaged ships in flooding condition, there are few comparative researches between the MPS and SPH methods. Souto-Iglesias et al. [21,22] investigated the consistency of MPS and discussed the differences with SPH. Several groups showed comparison results of the MPS and SPH methods for standard dam-break or sloshing tests [23, 24, 25]. Khayyer et al. [26,27] compared accuracy of both methods to compute fluid-structure interactions. Here, a systematic comparative study between the MPS and SPH methods is conducted on forced roll tests of a two-dimensional damaged compartment, and on a three-dimensional flooded compartment situation. Through comparison with dedicated experimental tests at model scale for various conditions, capability of the two particle methods to predict flooding flows is discussed and the accuracy of each particle method is carefully investigated. In a first stage the MPS and SPH methods are compared with each other in the two-dimensional situation without taking the air phase into account, showing discrepancies with the experimental results. The importance of the air phase was highlighted for flooding problems [28] and water slamming [29]. Thus in a second stage, it is shown how modeling the trapped air in damaged compartments permits to recover closely the experimental results. This is done in two different ways: either by numerically modelling the local equations in both phases or by using a simple Boyle's law model. Then, a complicated three-dimensional flow is simulated by the MPS and SPH methods and is compared with the experimental result in terms of hydrodynamic forces and flow configurations in the compartment. Finally, conclusions are drawn regarding the capabilities and differences of the two methods for investigating realistic complex geometry flooding situations.

The present paper is organized as follows. In section 2.1 and 2.2, a brief review of the MPS and SPH methods is provided and some details are given on the two related numerical solvers used for the comparison study. Experimental setup and measurement procedure used for the validation of these particle methods are shown in section 3.1 and 3.2. Comparison results between the MPS, SPH and experimental results are presented for the two-dimensional situation in section 4.1. The trapped air effect and its numerical treatment are studied in section 4.2. The results for a realistic three-dimensional flooding situation are described and discussed in section 4.3. Finally, the main conclusions of the paper are given in section 5.

2. MPS AND SPH METHODS

2.1 MPS solver

The moving particle semi-implicit (MPS) method was proposed by Koshizuka and Oka [30] for solving incompressible fluid flows. The governing equations used in the MPS method, dealing with incompressible flow approximation, are the incompressible Navier-Stokes equations written in Lagrangian formalism (Eq.1-3).

$$\left.\frac{D\rho}{Dt}\right|_i = 0 \tag{1}$$

$$\left.\frac{D\boldsymbol{u}}{Dt}\right|_i = -\frac{1}{\rho}\langle\nabla P\rangle_i + \nu\langle\nabla^2\boldsymbol{u}\rangle_i + \boldsymbol{g} \tag{2}$$

$$\left.\frac{D\boldsymbol{r}}{Dt}\right|_i = \boldsymbol{u}_i \tag{3}$$

In (Eq. 1-3), variables are the density ρ, time t, velocity $\boldsymbol{u}$, pressure P, kinematic viscosity coefficient ν, gravity acceleration $\boldsymbol{g}$ and position $\boldsymbol{r}$.

The spatial differential operators in (Eqs. 1-2) are discretized with the particle interpolations in (Eqs. 4-6), with use of a weighting function, $w(r)$, and summation over the neighbor particles j included in a compact neighborhood Ω_i around particle i. The inter-particle distance is denoted $r_{ij} = |\boldsymbol{r}_j - \boldsymbol{r}_i|$. Each particle represents a volumic fluid element (equivalent to a material cell in mesh-based methods).

$$\langle\nabla P\rangle_i = \frac{d}{n^0}\sum_{j\in\Omega_i, j\neq i}\left[\frac{P_j - P_i}{{r_{ij}}^2}(\boldsymbol{r}_j - \boldsymbol{r}_i)w(r_{ij})\right] \tag{4}$$

$$\langle\nabla^2\boldsymbol{u}\rangle_i = \frac{2d}{\lambda_i n^0}\sum_{j\in\Omega_i, j\neq i}\left[(\boldsymbol{u}_j - \boldsymbol{u}_i)w(r_{ij})\right] \tag{5}$$

$$\lambda_i = \frac{\sum_{j\in\Omega_i, j\neq i}{r_{ij}}^2 w(r_{ij})}{\sum_{j\in\Omega_i, j\neq i} w(r_{ij})} \tag{6}$$

d is the number of dimensions of the considered problem and n^0 is the particle number density in the initial configuration.

In the MPS method, the gravity and viscous terms in (Eq. 2) and the flow kinematics (Eq. 3) are evolved explicitly in time, and the Pressure Poisson Equation (Eqs. 7-8) is solved implicitly, i.e. we have a semi-implicit time stepping:

$$\langle\nabla^2 P\rangle_i^{n+1} = \frac{2d}{\lambda_i n^0}\sum_{j\in\Omega_i, j\neq i}\left[\left(P_j^{n+1} - P_i^{n+1}\right)w(r_{ij})\right] = -\frac{\rho}{\Delta t^2}\frac{n_i^* - n_0}{n_0} \tag{7}$$

$$n_i^* = \sum_{j \in \Omega_i, j \neq i} w(r_{ij}^*) \tag{8}$$

where P^{n+1} is the pressure at next time step to be solved implicitly, Δt the time step, n_i^* the intermediate step particle number density and $\boldsymbol{r}_i^*$ the intermediate step particle position. Once the pressure known, its gradient is calculated by (Eq. 4) and is used to update the position of particles while satisfying the incompressibility assumption (Eq. 1).

An in-house solver based on the MPS method, named MPS-Hydro, is used for the MPS simulations (see [31,32] for the algorithm of the solver). The weighting function used in this study is the one of (Eq. 9), with r_e the effective radius. It is modified from the conventional one [30] to have a finite value even when the effective radius goes to zero.

$$w(r) = \begin{cases} \left(\frac{r_e}{(r + 0.05 r_e)} - 1\right) - \left(\frac{r_e}{(r_e + 0.05 r_e)} - 1\right) & 0 \leq r < r_e \\ 0 & r_e \leq r \end{cases} \tag{9}$$

In MPS-Hydro, wall boundaries are imposed by mirror-particles [17,32] and the wall reflection algorithm which inverts the velocity vector of a fluid particle when it comes within the threshold of minimum distance to the wall surface. The compressibility of fluids [33] and quasi-compressibility [34] are introduced in solving the Pressure Poisson Equation to stabilize the calculation.
During the last decade the MPS method has been largely improved, especially solving the free-surface instability which was the recognized defect of the standard MPS method, see, e.g., [35].

2.2 SPH solver

The Smoothed Particle Hydrodynamics (SPH) method [36,37] was first applied to free-surface flows by Monaghan [38]. Differently from the MPS where we make the incompressible flow assumption, the weakly-compressible approach is used in the original SPH framework to solve the Navier-Stokes equations (Eqs. 14-15), with a closure barotropic equation of state (Eq. 16).

$$\left.\frac{D\rho}{Dt}\right|_i = -\rho_i \langle \nabla . \boldsymbol{u} \rangle_i \tag{14}$$

$$\left.\frac{D\boldsymbol{u}}{Dt}\right|_i = -\frac{1}{\rho_i} \langle \nabla \mathrm{p} \rangle_i + \nu \langle \nabla^2 \mathbf{u} \rangle_i + \boldsymbol{g} \tag{15}$$

$$p_i = \frac{\rho_0 c_0^2}{\gamma} \left[\left(\frac{\rho_i}{\rho_0} \right)^{\gamma} - 1 \right] \tag{16}$$

where γ is the polytropic coefficient (set to 7 for water).
In the weakly-compressible approach, the sound speed is artificially lowered to save computational

time (up to the limit where the Mach number *Ma* is equal to 0.1; *Ma* is based on a reference velocity derived here from a Froude number equal to unity ($v_0 = \sqrt{gH}$) and the reference length H equal to domain depth), without influencing the incompressible part of the flow at aim in our problems [39]. The weighting function w chosen in the present SPH scheme is the Wendland kernel [40]:

$$w(r) = \frac{7}{\pi}\begin{cases}\left(1-\frac{r}{r_e}\right)^4\left(1+4\frac{r}{r_e}\right) & 0 \le r \le r_e \\ 0 & r_e \le r\end{cases} \tag{17}$$

The classical SPH space operators applied to pressure gradient, velocity divergence and velocity Laplacian (discretized after Monaghan [40]) lead to:

$$\langle \nabla P \rangle_i = \sum_{j\in\Omega_i}\left[\left(P_j + P_i\right)\nabla w\left(r_{ij}\right)V_j\right] \tag{18}$$

$$\langle \nabla . \boldsymbol{u} \rangle_i = \sum_{j\in\Omega_i}\left[\left(\boldsymbol{u}_j - \boldsymbol{u}_i\right).\nabla w\left(r_{ij}\right)V_j\right] \tag{19}$$

$$\langle \nabla^2 \boldsymbol{u} \rangle_i = \sum_{j\in\Omega_i}\left[\frac{\left(\boldsymbol{r}_j - \boldsymbol{r}_i\right).\left(\boldsymbol{u}_j - \boldsymbol{u}_i\right)}{r_{ij}^2}\nabla w\left(r_{ij}\right)V_j\right] \tag{20}$$

where V_i is the volume of particle i. However, this naive fully-explicit SPH implementation (called the strong formulation) into the previous system (Eqs. 14-15) leads to unstable formulation. A simple way to stabilize it is to add an artificial viscosity, but pressure field may be noisy. A more accurate alternative is to rewrite the equations in conservative form and to derive a weak formulation of the system (Eqs. 14-15) based on a Finite Volume numerical analysis (see [42]) and a Riemann solver. This leads to the following discrete system [42, 43] for the inviscid part of the system (hyperbolic Euler equations):

$$\frac{dV_i\Phi_i}{dt} = \sum_{j\in\Omega_i}\left[2\mathbf{G}\left(\Phi_i, \Phi_j, \boldsymbol{n}_{ij}\right)\nabla w\left(r_{ij}\right)V_jV_i\right] + V_i\boldsymbol{S} \tag{21}$$

where Φ_i is the vector of conservative variables: $\Phi = (\rho, \rho u)^t$. $\boldsymbol{G}$ is the flux solution (for both continuity and momentum equations) of the Riemann problem based on left Φ_i and right Φ_j states corresponding to particles i and j, and along direction $\boldsymbol{n}_{ij} = \nabla w_{ij}/\left\|\nabla w_{ij}\right\|$. In the present work, this function $\boldsymbol{G}$ is based on an approximate Riemann solver called acoustic, and its accuracy is enhanced

with the MUSCL scheme. $\boldsymbol{S}$ is the vector of source terms, including gravity and viscous effects.

Besides, in this specific formulation of SPH it is needed to evolve in time the volume of each particle. An equation similar to the continuity equation is used and discretized as follow:

$$\frac{dV_i}{dt} = \sum_{j \in \Omega_i} [(\boldsymbol{u}_j - \boldsymbol{u}_i).\nabla w(r_{ij}) V_j V_i] \quad (22)$$

Time forwarding of both (Eq. 21) and (Eq. 22) is explicit and is based on a Runge-Kutta scheme (of 4th order).

The SPH solver used in this study is SPH-Flow. Boundary conditions are enforced by a Boundary Integral Method with CutFace Approach (BIM-CFA) [44] which requires neither particles on the boundary nor ghost particles. This method reduces implementation complexity and allows to simulate more easily complex geometries. Special care is taken for the parallel implementation of the whole SPH scheme to keep an efficient scalability (almost perfect up to tens of thousands of cores [45]).

2.3 Comparison of MPS and SPH features to study flooding

In previous paragraphs, both particle methods were introduced with their respective main features. To underline which ones are specific to study flooding scenarios, the following Table 1 sum-up these characteristics.

Table 1: Features for flooding simulations

Features	MPS	SPH
Solid boundaries	Mirror-particles [17,31]	Integral approach (BIM-CFA) [44]
Total force calculation	Pressure integration on solid boundaries [31]	Pressure integration on solid boundaries with integral approach (BIM-CFA) [44]
Free-surface handling	Conventional method using	Naturally handled by the

	the free surface parameter [30]	method [46]
Two-phase modeling (details in section 4.2)	Local modification of free-surface boundary condition to handle over-pressure from trapped air pocket	Full discretization of air phase [47]

3. MODEL-SCALE EXPERIMENT

The nonlinear behavior of a damaged ship in serious flooding situations is so complicated that it is difficult to directly compare the MPS and SPH methods in time history of ship motion. In that sense, sophisticated situation/experiment is preferable at first for the validation of the particle methods and for the comparative study between the MPS and SPH methods, so that prescribed forced roll tests are conducted instead of water flooding tests. Model-scale experiments for investigating the validity of the numerical methods are performed for a simple two-dimensional damaged model and a realistic three-dimensional flooded model.

3.1 Two-dimensional damaged model

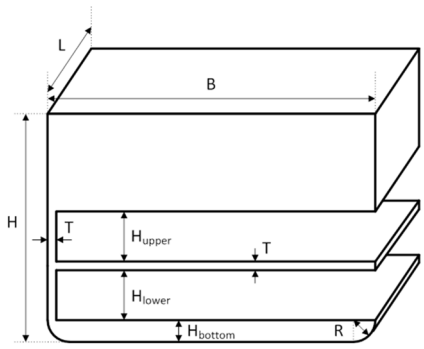

Fig. 1: 2-D damaged compartment model (front and rear broadsides not represented)

For the comparison between MPS and SPH methods, a two-dimensional model of a damaged car deck section is selected. A schematic view of the model is given in Fig.1 and its dimensions are shown in Table 2.

Table 2: Dimension of the model (2-D)

B	H	H_{bottom}	H_{lower}
0.5 m	0.35 m	0.035 m	0.085 m
H_{upper}	L	R	T
0.085 m	0.28 m	0.035 m	0.008 m

The model was made by acrylic with thickness of 0.008m. The model has upper and lower compartments and monotonous side damage is presented along the right broadside for both compartments. Front and rear broadsides are kept closed by acrylic walls (not represented in Fig. 1). Forced roll tests were conducted at a two-dimensional wave basin at Osaka University. The experimental setup is shown in Fig. 2.

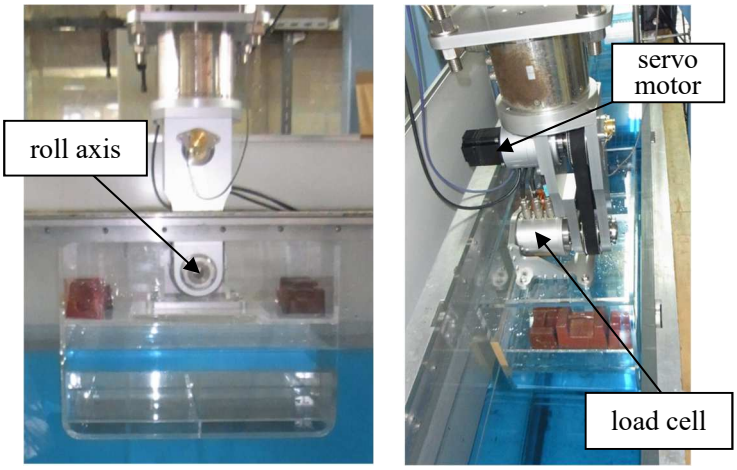

Fig. 2: Experimental setup (2-D)

A rotating moment is added by an electric servo motor through a driving belt with a feedback control. The horizontal and vertical forces and the moment around the center of rotation are measured by a load cell rotating together with the model. The measurement axis of the roll moment coincides with the rotation axis, and hence the roll moment around the center of rotation can be directly measured. The height of roll axis is 0.3m from the bottom of model. A pressure sensor with diameter of 1 cm is installed on the inner sidewall at (x, y) = (-0.242m, 0.160m). The sampling rate for the measurement is 100 Hz. The test conditions are shown in Table 3.

Table 3: Test conditions (2-D)

damage opening	amplitude: ϕ_a (deg)	period: T_ϕ (s)	draft: d (m)
upper deck	20	2.5	0.146
upper & lower decks	20, 30	2.5	0.146

The roll period is decided from the designed natural roll period of a PCTC. The body-fixed coordinate system (Fig. 3) is used for the analysis of forced roll test. The moment of inertia of the model and measurement system is omitted by subtracting the forced roll test result in the air conducted with the same amplitude and period.

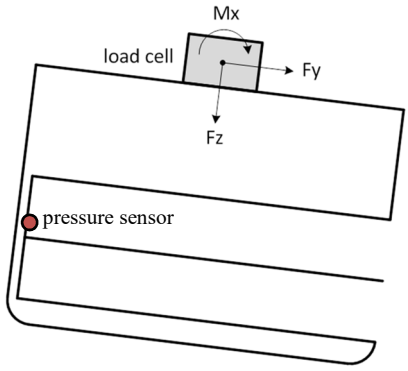

Fig. 3: Coordinate system for the forced roll test (2-D)

3.2 Three-dimensional flooded model

In order to investigate the validity of the studied particle methods for complex flows in realistic situations, a three-dimensional compartment of a PCTC is then used. This model is one of the sub-divisions of a car hold and ramp slopes connecting each floor are present as shown in Fig.4.

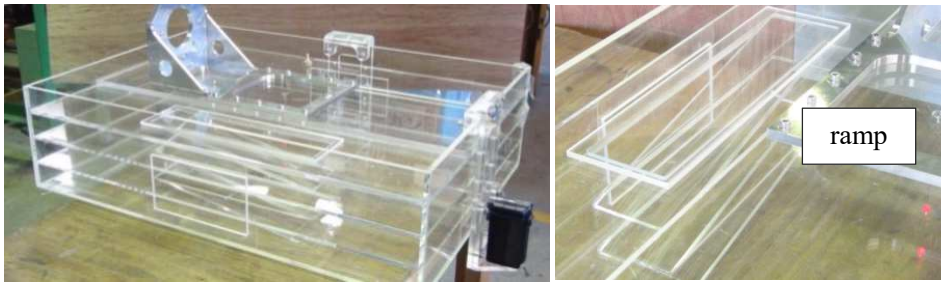

Fig. 4: Three-dimensional compartment model

The model was made by acrylic with thickness of 0.008m except for the ramp and deck floors. The principal dimensions of the three-dimensional model are described in Fig. 5.

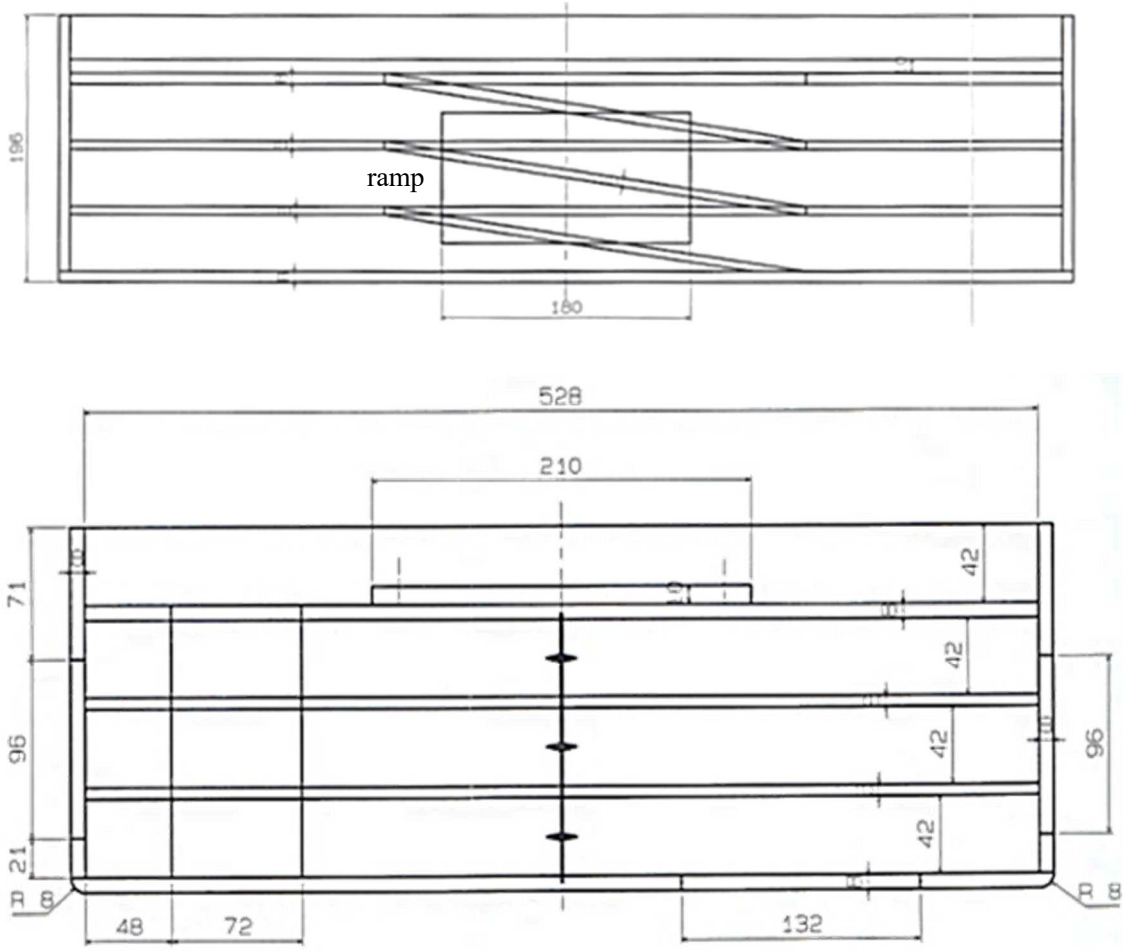

Fig. 5: Dimensions of the model (3-D) in millimeters

Forced roll tests were conducted at a towing tank of Osaka University. Fig. 6 shows a photo of the experimental setup.

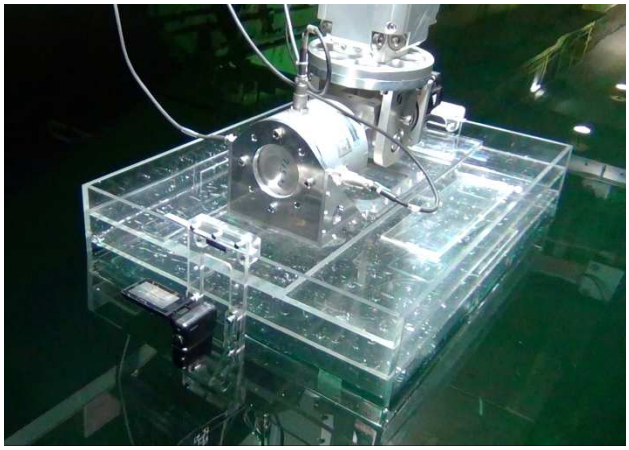

Fig. 6: Experimental setup (3-D)

These experiments were conducted using a different set of driving-motor and load cell from the two-dimensional test, but the principle of the experiment/measurement is same. The forced roll tests for the three-dimensional model were performed with a certain amount of floodwater but without damage openings. The tested condition is shown in Table 4.

Table 4: Test condition (3-D)

amplitude: ϕ_a (deg)	period: T_ϕ (s)	draft: d (m)	height of x-axis (m)
20	2.8	0.07	0.164

The body-fixed coordinate system is used for the analysis of hydrodynamic forces as in the two-dimensional cases, see Fig. 7. The forced roll tests were repeated for the empty and partially filled conditions. The measured hydrodynamic force without floodwater is subtracted from that with floodwater to extract the hydrodynamic force produced by the floodwater, to be directly compared with MPS and SPH calculations.

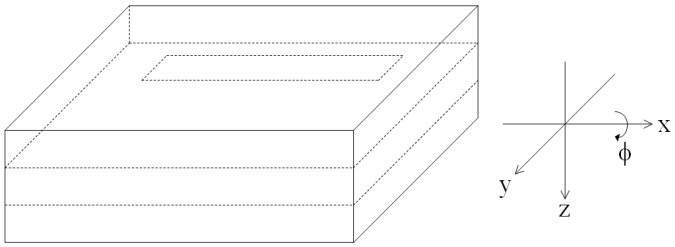

Fig. 7: Coordinate system for the forced roll test (3-D)

4 NUMERICAL RESULTS

4.1 Two-dimensional damaged model

The geometry adopted to numerically represent the test configuration is presented in Fig. 8. This numerical tank is composed of straight beaches. This simple geometry is adopted to reduce wave reflections from the ends of the tank and to ease the comparison of flow solvers. More efficient beaches could be implemented but may require more complex tuning depending on particle methods. Fluid viscosity is neglected in both numerical solvers, which is a reasonable assumption when modeling such fast dynamics flows.

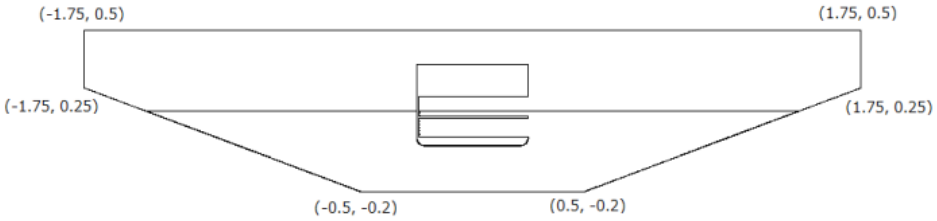

Fig. 8: Numerical tank configuration

The same initial inter-particle distance *dx* (of 0.0015 m) is used for both the MPS and SPH calculations, which leads to about 300,000 water particles. Numerical parameters used in each flow solver are shown in Tables 5-6. In the MPS calculation, the ratio of effective radius and initial inter-particle distance, r_e/dx, of 2.1 and 4.0 are used for the particle number density and the gradient operator, and the Laplacian operator, respectively.

Table 5: Simulation parameters (MPS-Hydro)

time step (s)	ratio r_e/dx	multiplication coefficient [34]
0.0002 - 0.00025	2.1 & 4.0	1.01

Table 6: Simulation parameters (SPH-flow)

Courant number	speed of sound	ratio r_e/dx
0.375 (Runge-Kutta 4)	20 m/s	4.0

The forced roll motion is prescribed with a sinusoidal function (Eq. 23). In numerical simulations, it is represented by imposing velocities to the wall particles/elements forming the damaged body. The velocities can be obtained as the differential of the sinusoidal function.

$$\phi = \phi_a sin\left(\frac{2\,\pi}{T_\phi} t\right) \tag{23}$$

Comparisons in time series of hydrodynamic force and local pressure between the experimental and numerical results of MPS and SPH methods are presented in Fig.9-11, for single-phase simulations as a first stage.

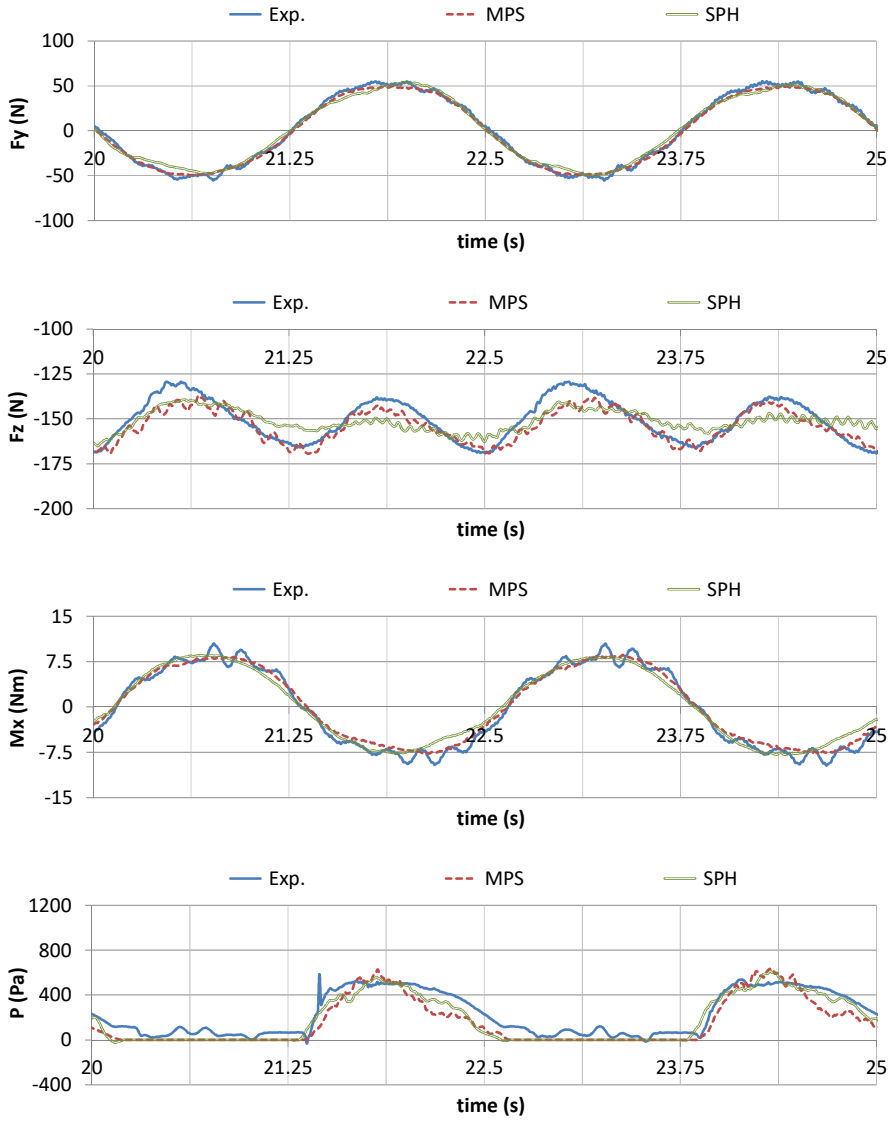

Fig. 9: Comparison of hydrodynamic forces, moment and relative pressure for one-compartment damage condition with ϕ_a = 20 deg, T_ϕ = 2.5 s. Numerical results are for single-phase simulations.

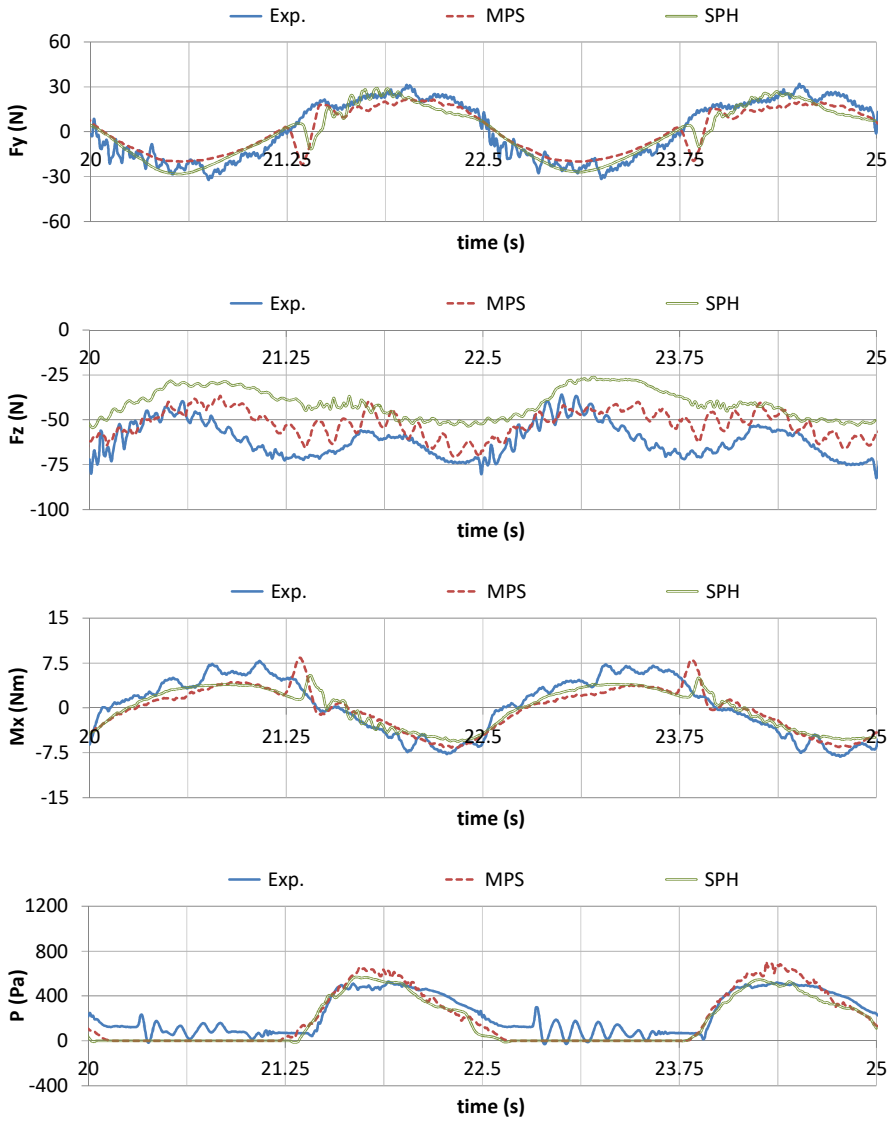

Fig. 10: Comparison of hydrodynamic forces, moment and relative pressure for two-compartment damage condition with $\phi_a = 20$ deg, $T_\phi = 2.5$ s. Numerical results are for single-phase simulations.

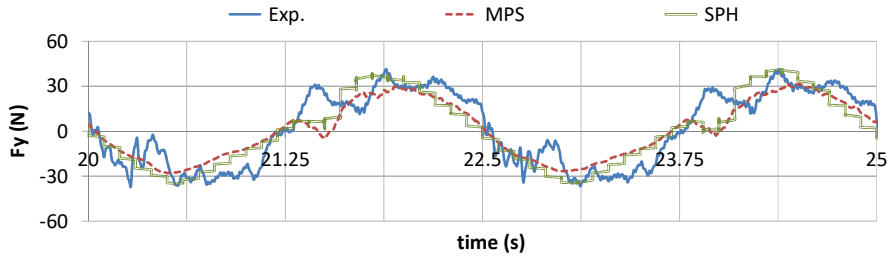

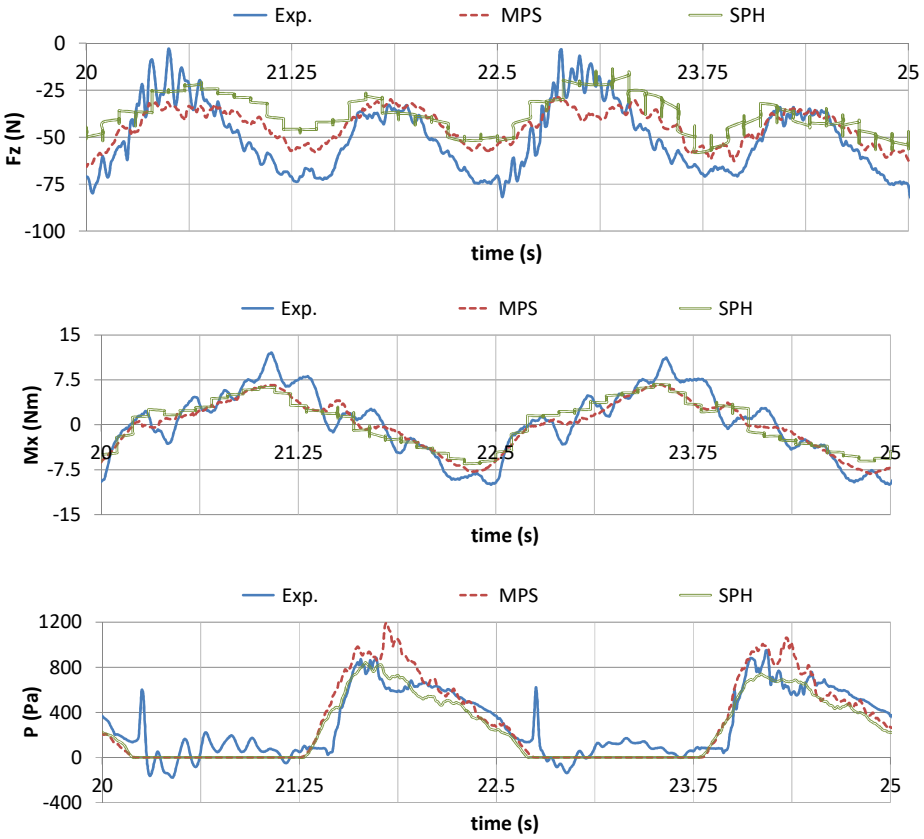

Fig. 11: Comparison of hydrodynamic forces, moment and relative pressure for two-compartment damage condition with ϕ_a = 30 deg, T_ϕ = 2.5 s. Numerical results are for single-phase simulations.

Here the numerical results by MPS-Hydro and SPH-flow are smoothened by a simple moving average method with the time interval of 0.1 s for the hydrodynamic forces and of 0.02 s for the pressure according to the low-pass filter used in the experiment. Moreover, since we are interested in periodic movement rather than in transient stage, we average data over last periods (six last for computations and eight last for experiments) for comparisons (see Appendix A). For the case of one-compartment damage, the MPS and SPH methods can represent the model experiment quantitatively in F_y and M_x, while do qualitatively in F_z and pressure. Both particle methods show quite similar results, from a view point of engineering use, and a certain difference can be seen in the amplitude of F_z. For the cases of two-compartment damage situation, the prediction accuracy of both particle methods becomes generally worse than that of one-compartment damage situation. In the case with the roll amplitude of 20 degrees, the spiky drop/rise appears in F_y and M_x around t = 21.4 s and t = 23.9 s and successive vibrations occur after that time. Similar tendency is not found in F_z and pressure. The shift of average value is found in F_z in numerical results. Recalling that both experiments and simulations are one-way coupling between ship motion and fluid response, one of the possible reasons of these discrepancies is the use of smaller depth for the numerical tank as compared to the experiment. The numerical

oscillation of the MPS result is more significant than that of the SPH one in F_z while experimental oscillation amplitude is in between these two numerical oscillation amplitudes. In the case with the roll amplitude of 30 degrees, similar trend can be observed as for the ϕ_a = 20 deg case, the overall prediction accuracy of numerical results for ϕ_a = 30 deg is slightly better than that for ϕ_a = 20 deg even though the water behavior becomes more violent with the increase of roll amplitude.

In all the tested conditions, it is difficult to find quantitative differences between the MPS and SPH methods in the previous force and pressure signals. Despite this apparent similarity, several discrepancies exist when the numerical results are carefully compared with the experimental ones, in the two-compartment damage case. They are found in the amplitude of M_x, the average of F_z and the pressure oscillation when closing to zero. In order to clarify the reason of these discrepancies, visual comparison of the fluid motion in the compartments is performed. Fig. 12 shows the comparison for the two-compartment damage case with roll amplitude of 20 degrees, where the worst agreement in hydrodynamic forces is found. Numerically predicted free-surface shapes at different instants of the cycle globally look nicely similar to each other. However, they are different from the experimental result in some phases. The snapshots of the experiment clearly show the presence of trapped air in the lower compartment. With the single-phase modeling adopted both in the MPS and SPH methods in a first stage, this trapped air is missing which, consequently, leads to different ulterior evolution of the flow in this lower compartment which, in turn, may explain the discrepancy in the hydrodynamic force and pressure mentioned above.

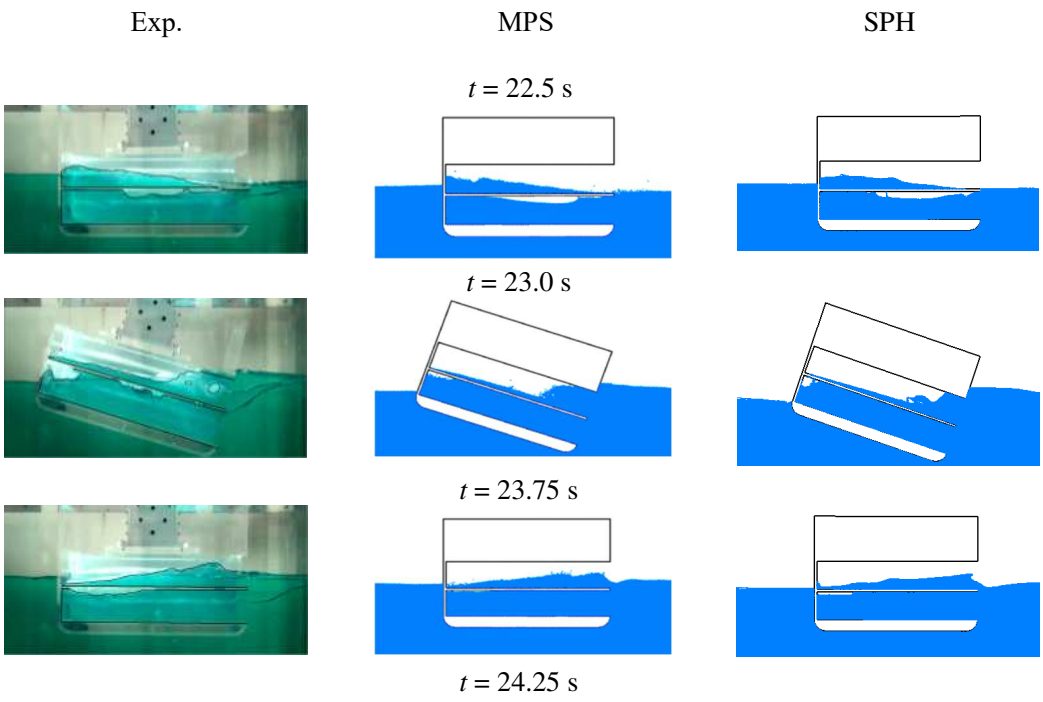

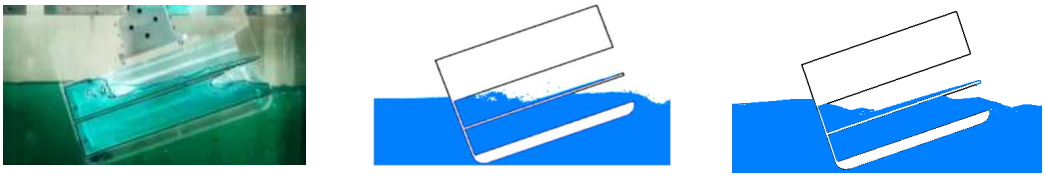

Fig. 12: Comparison of floodwater situation with $\phi_a = 20$ deg, $T_\phi = 2.5$ s. Numerical results are for single-phase simulations.

Regarding execution times of both methods in the present context, we can draw similar conclusions as observed for SPH method. Using an incompressible semi-implicit method permits in practice a gain up to 10 in terms of time steps compared to its explicit weakly-compressible counterpart (this gain is linked to artificial Mach number, 0.1: in implicit method, time step can be driven only by convective velocity which is ten times higher than speed of sound). However this gain is counterbalanced by the additional cost of solving the Pressure Poisson Equation (Eqs. 7-8) and imposing the Dynamic Free-Surface Boundary Condition. So we found very comparable CPU costs for both methods, SPH and MPS, in the end for present single-phase application.

4.2 Trapped air modeling

From the comparisons in Section 4.1, the existence of trapped air in the compartment could be the reason of discrepancies between the particle methods and experiment, mainly existing in the two-compartment cases studied. Therefore, in a second stage we accounted for the trapped air effect with different approaches in the MPS and SPH methods as follows.

In MPS-Hydro, the trapped air is assumed to be a single-air pocket and the instantaneous pressure of the compressed air is calculated by Boyle's law. For the numerical implementation, percentage of water particles present at the entrance of the lower damage opening is monitored and used for the judgement whether the lower damage opening is fully submerged or not (i.e. whether the air inside will be trapped or escape to the outside). When it is submerged, the instantaneous air volume (area in two-dimensional case) is measured based on water particle presence in the compartment. It is assumed the shape of trapped air when the compartment just gets submerged is circular and the initial pressure can then be determined as the average hydrostatic pressure at the depth of circle center. The time-dependent pressure of the trapped air is then calculated based on Boyle's law (cf. Eq. 24) and it is imposed to free-surface particles and non-wetted wall particles when solving the pressure Poisson equation until the lower damage opening partially exposes to the air. This partial exposure is defined as the existence ratio of water is 80% or less in this study.

$$P_a(t) = P_{a0}\frac{A_0}{A(t)} \tag{24}$$

where P_a, P_{a0}, A, A_0 denote air pressure, initial air pressure, area of trapped air, initial area of trapped air (in 2-D, otherwise the circle becomes a sphere and the area a volume).

Once it emerges, zero pressure is imposed to the free-surface particles as usual manner. With use of Boyle's law, the effect of air entrapped in the damaged compartment can be considered in a single-phase simulation. It should be noted that with this strategy the CPU cost does not increase because the air pressure is easily imposed to the free-surface particles instead of zero pressure as Dirichlet condition. Of course the counterpart is that this modeling is approximate compared to the actual real two-phase evolution.

Within SPH-flow, the approach to model trapped air is indeed different: the choice is made to fully simulate the air phase presence, as in the literature [48], by solving the two-phase Navier-Stokes equations. Thus an additional set of particles is required to discretize the air domain. These particles evolve in time with the same SPH system of equations (Eqs. 21-22) as water particles but the equation of state (Eq. 16) for this gas phase is set with appropriate parameters (polytropic coefficient γ equal to 1.4 and adequate speed of sound to reproduce air compressibility and to be able to describe properly situations where air bubbles are trapped [49]). Special treatment to ensure mass conservation is also performed at the interface to be compatible with the use of a Riemann solver [47]. Surface tension effects are not taken into account in the present case due to the rather large scales involved. In order to avoid excessive computational time, the speed of sound of air is artificially decreased to 50m/s. Real compressibility of air is no more respected but compared to actual convective velocities in the air, this condition ensures a weak-compressibility assumption.

Note that air phase is modelled by a simple air pocket model in MPS (only its surface area is a matter of importance while air pocket has no velocity) while interface jump conditions are applied locally in SPH allowing to solve the flow equations everywhere in air phase (inside and outside air pocket). Note also that Boyle's law (in MPS) is an isentropic law while Tait's equation of state (in SPH) is adiabatic, which could result in slight discrepancies during compression or expansion of high intensity which is not expected in the present study.

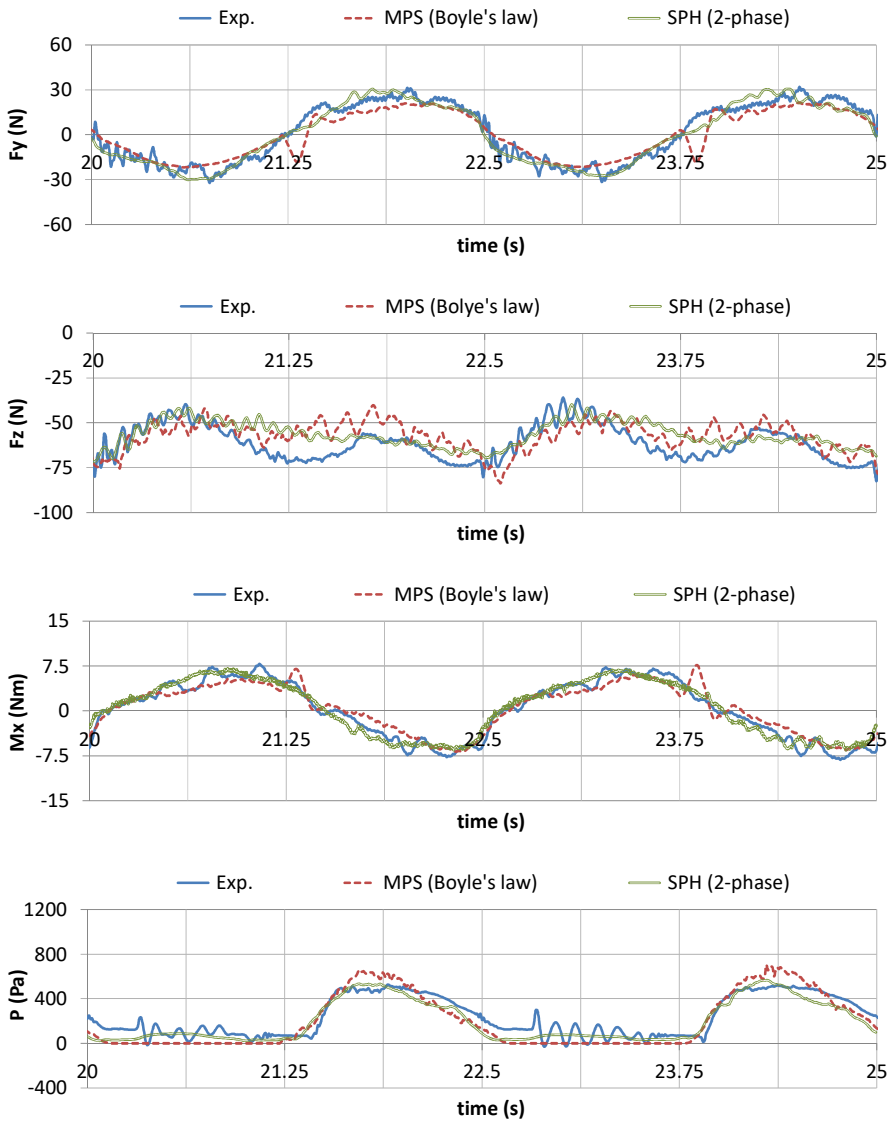

Fig. 13: Comparison of hydrodynamic forces, moment and relative pressure for two-compartment damage condition with $\phi_a = 20$ deg, $T_\phi = 2.5$ s. Numerical results include partly (MPS) or fully (SPH) the air phase.

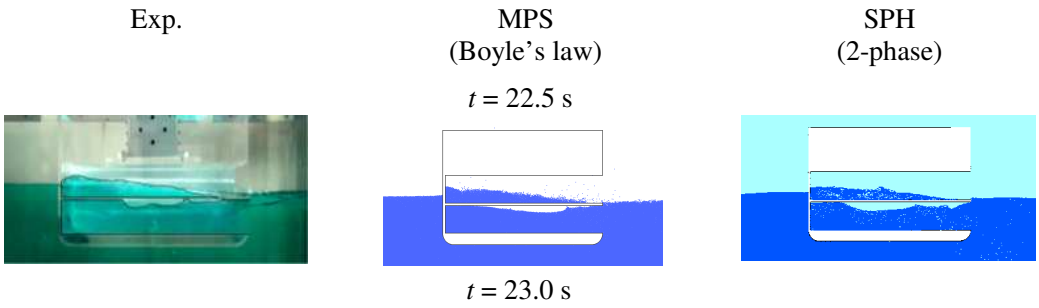

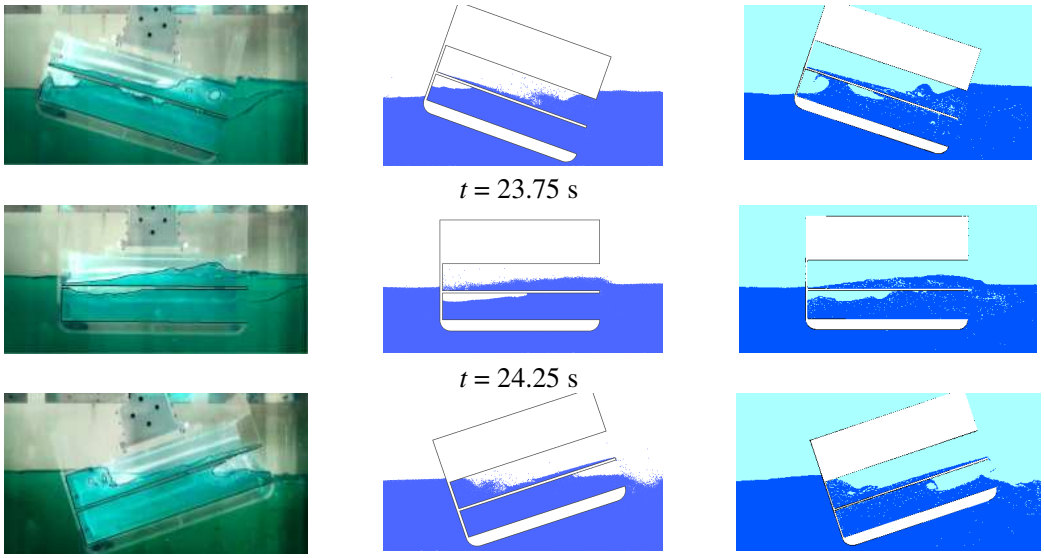

Fig. 14: Comparison of floodwater situation with ϕ_a = 20 deg, T_ϕ = 2.5 s. Numerical results include partly (MPS) or fully (SPH) the air phase.

Figs. 13-14 show the comparison result between the MPS with Boyle's law simulation, the two-phase SPH simulation and the experiment. Here the two-compartment damage case with ϕ_a = 20 deg is selected, where the trapped air might be most influential on the hydrodynamic force. The spiky drop/rise found in Fig.10 completely disappears in the SPH result, while does not in the MPS result. The two-phase SPH agrees with the experimental result quantitatively in F_y, M_x and pressure, and significant improvement is also confirmed in F_z. It is noted that the shape of air-water interface and air-water mixture are well captured and the calculated pressure of air-pocket agrees with the experimental result averagely, as is visible in the pressure signal where the plateaus (e.g. between t = 22.6 s and t = 23.8 s) correspond to periods of time where the pressure sensor is in the air pocket. The presence of the trapped air can be also represented by the MPS with Boyle's law model and the prediction accuracy is well improved, but the numerical result agrees qualitatively while the two-phase SPH does quantitatively. However, the simple treatment of the air in MPS could be useful for practical uses because the trapped air effect can be considered without increasing the CPU cost. There is still certain discrepancy in F_z between the experiment and the numerical results even taking account of trapped air. This might be because the numerical beach does not damp enough reflected waves which interfere with the floodwater in the compartment. Therefore, further improvement is expected if a larger numerical tank equipped with efficient beaches was used. The pressure fields at t = 23.0 s and t = 23.75 s are shown in Fig.15, which are calculated by the MPS with Boyle's law model. These snapshots tell that the uniform non-zero pressure is appropriately imposed to the free-surface particles and non-wetted wall particles of the trapped air pocket.

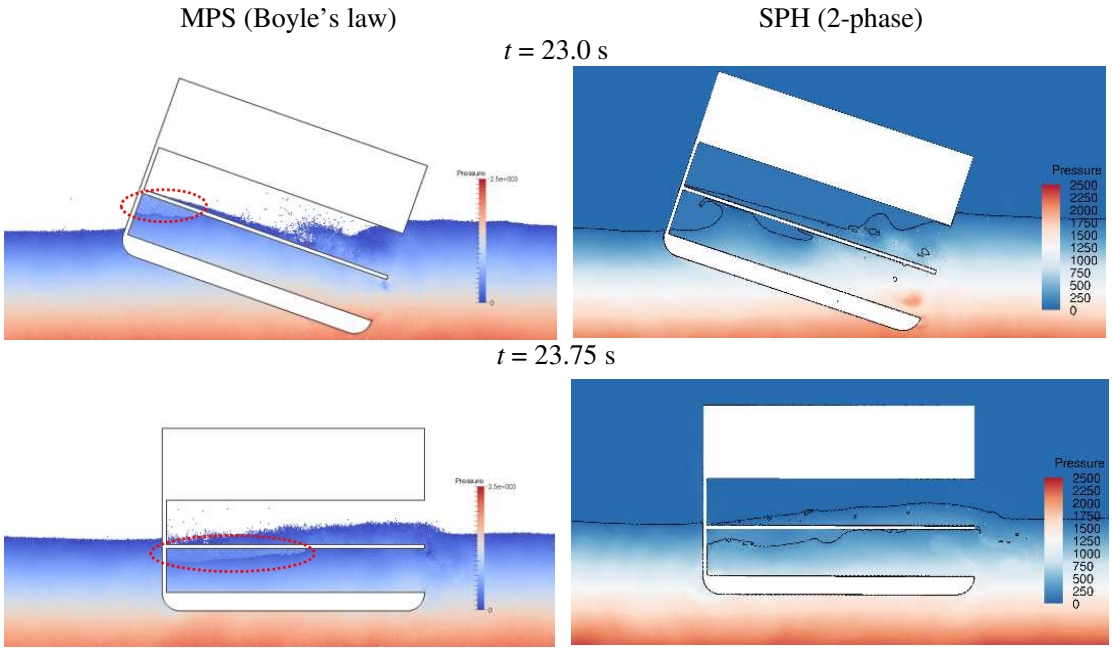

Fig. 15: Pressure field in MPS and SPH simulations, at t = 23.0 s (top) and at t = 23.75 s (bottom). For SPH result, black markers correspond to air-water interface.

4.3 Three-dimensional flooded model

Finally, 3-D forced roll simulations are performed by the MPS and SPH solvers, with the same condition as the experiment, to investigate the validity and accuracy of the particle methods for three-dimensional complex flows in a realistic configuration. Calculation conditions used in MPS-Hydro and SPH-flow are shown in Tables 7-8.

Table 7: Simulation parameters (MPS-Hydro)

Initial dx [m]	0.006	0.003
Time step [s]	0.00075	0.000625
Multiplication coefficient [34]	1.01	1.01
Number of wall particles	101305	449542
Number of water particles	105216	842976

Table 8: Simulation parameters (SPH-flow)

Initial dx [m]	0.006	0.003
Number of water particles	104932	837891
Ratio r_e/dx	2.459	

Speed of sound [m/s]	20
Courant number	0.375

Here both simulations are performed with different inter-particle distances to check the influence of spatial resolution on the result. The thickness of the ramp and deck floor is 6 mm, so the maximum inter-particle distance should be quite smaller than this value if ghost particles were used for wall boundary condition. However, both in MPS-Hydro and SPH-flow codes we can use an inter-particle distance of 6 mm, same value as the minimum thickness of the model, thanks to the mirror-particles wall boundary condition in MPS and BIM-CFA method in SPH-flow.

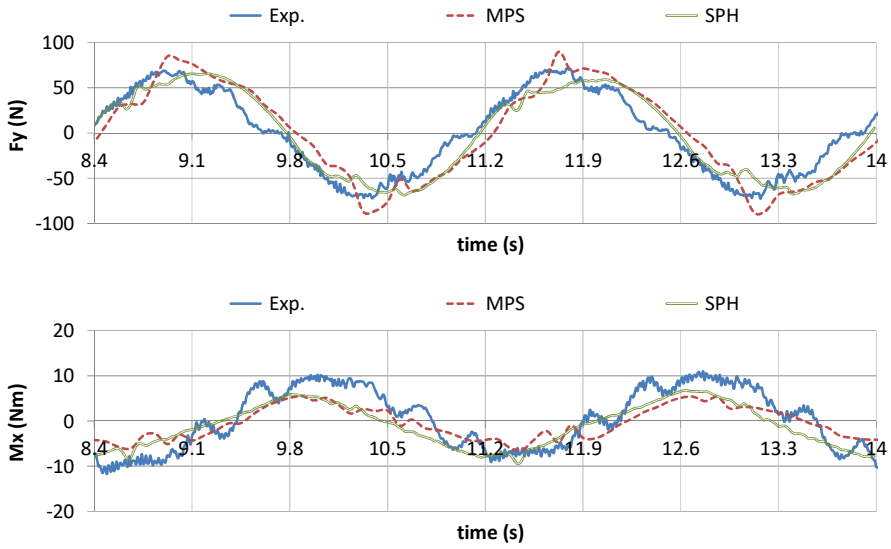

Fig. 16: Comparison of hydrodynamic force and moment with ϕ_a = 20 deg, T_ϕ = 2.8 s. Numerical results are for single-phase simulations, with dx=6.0mm.

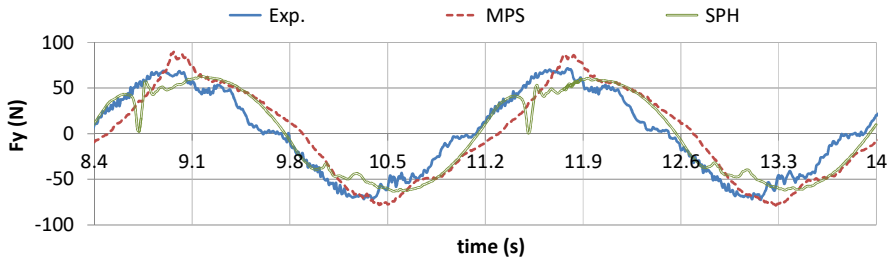

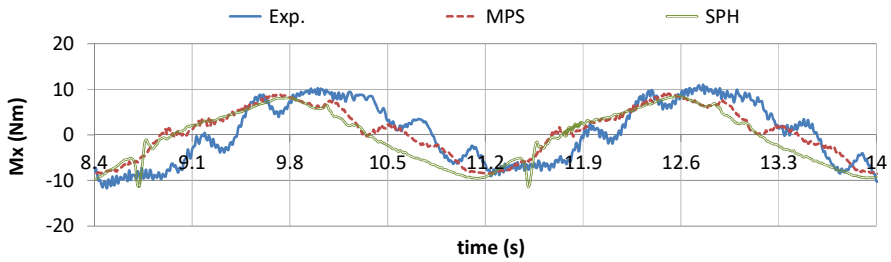

Fig. 17: Comparison of hydrodynamic force and moment with ϕ_a = 20 deg, T_ϕ = 2.8 s. Numerical results are for single-phase simulations, with dx = 3.0 mm.

The comparisons of hydrodynamic force between the two particle methods and the experiment are shown in Figs. 16-17, for the inter-particle distances of 6 mm and 3 mm, respectively. It is observable that both particle methods show similar trend, as it was the case for the two-dimensional cases. The finer resolution using the smaller dx shows better agreement with the experiment in the hydrodynamic force, and the estimated amplitudes of F_y and M_x are generally acceptable. However, discrepancy can be found in their phase. This might be because the effect of air movement is neglected in these three-dimensional simulations. Two-phase flow simulations or the Boyle's law approach, presented in section 4.2, might be a solution to improve this phase difference. Visual comparisons of the floodwater flow in the compartment are shown in Figs. 18-19 for the case of inter-particle distance of 3 mm. The existence of upwards and downwards flows along the ramp way is confirmed in both the MPS and SPH methods, in agreement with the experiment. In the MPS result, hoping of the particles near the free-surface is prominent. This result indicates the free-surface condition used in the MPS method needs to be improved. In the physical test, wave breaking beside the side walls and fragmentation of water on the ramps happen, and the MPS and SPH methods have no difficulty to reproduce these nonlinear flows.

Exp. MPS SPH

t = 8.4 s

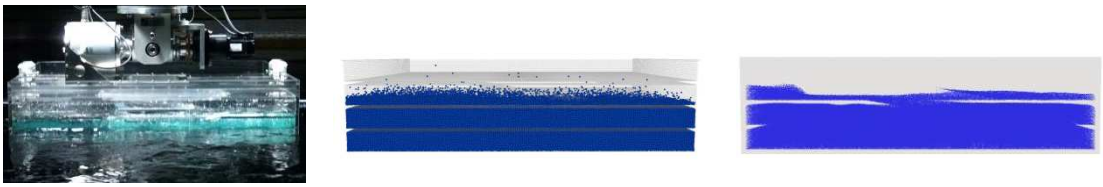

t = 8.96 s

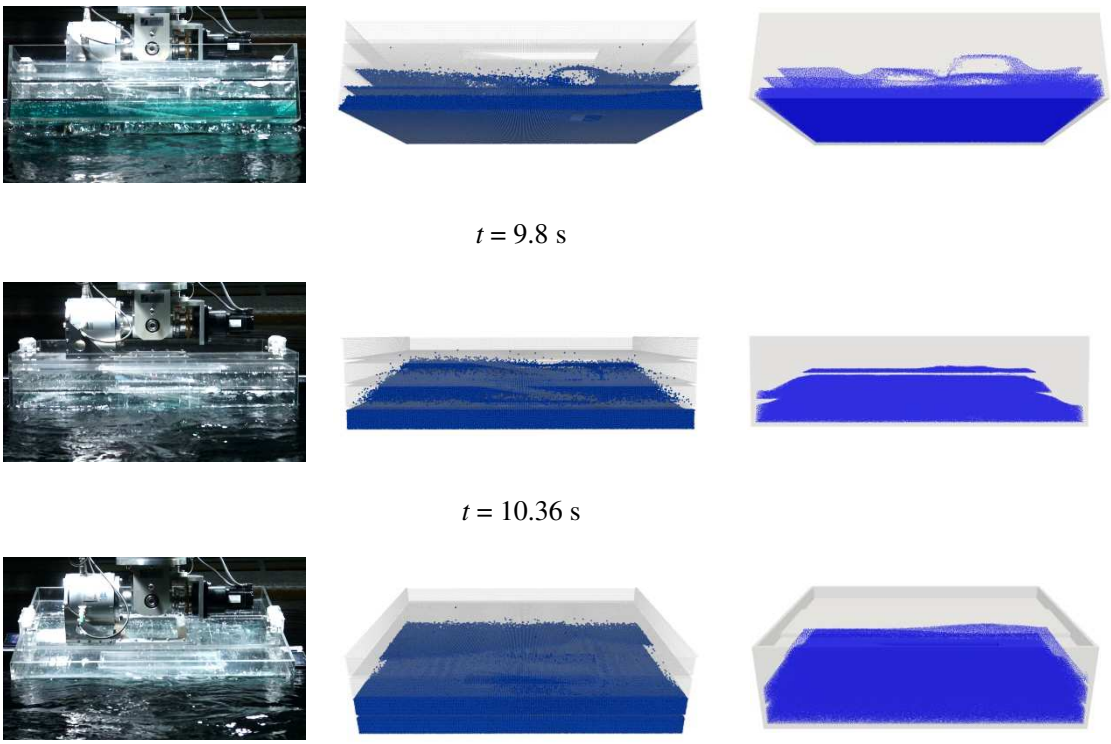

t = 9.8 s

t = 10.36 s

Fig. 18: Side views of floodwater situation. Numerical results are for single-phase simulations, with dx = 3.0 mm.

Exp. MPS SPH

t =8.4 s

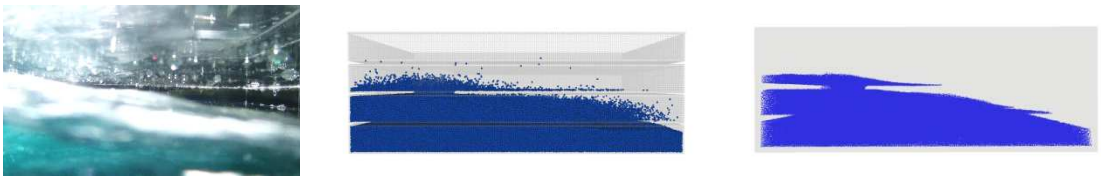

t =8.96 s

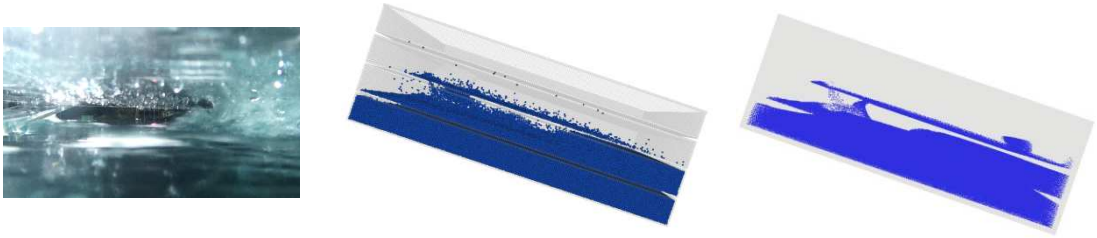

t = 9.8 s

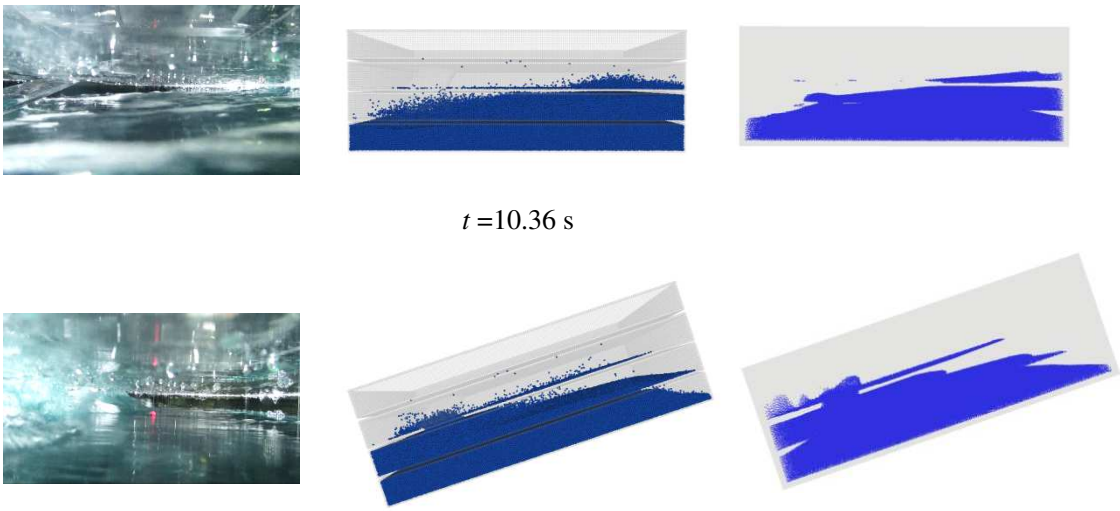

Fig. 19: Inside views of floodwater situation (2nd floor). Numerical results are for single-phase simulations, with dx = 3.0 mm.

5 CONCLUSIONS

In order to investigate the capability of particle methods for ship flooding problems, systematic comparisons between the MPS and SPH methods are performed on forced roll tests of a two-dimensional damaged and a three-dimensional flooded compartments. For the two-dimensional situations, it is demonstrated that the MPS and SPH methods, using the same inter-particle distance and numerical tank definition, show high similarity in general for all the tested conditions. Although there are minor differences between the two methods in the hydrodynamic force and local pressure, it is difficult to exhibit a ranking of the MPS and SPH methods from comparison results with the experiment. Actually, in single-phase simulations both particle methods are in good agreement with the experiment when trapped air effect is negligibly small. When trapped air is present with a significant role, the two-phase SPH model still provides accurate result in close agreement with the experiment, while the MPS model with Boyle's law yields only a qualitative agreement but without increasing the CPU cost with respect to single-phase simulation. The comparison of the MPS and SPH method is also made for a three-dimensional realistic flooded compartment, and the capability of the particle methods for simulating complex floodwater flows is demonstrated.

ACKNOWLEDGEMENT

This work was supported by a Grant-in Aid for Scientific Research of the Japan Society for Promotion of Science (No.25289317) and by the Japan Society for the Promotion of Science under the strategic young researcher overseas visits program for accelerating brain circulation on “International Collaboration on Strongly Nonlinear Fluid-Structure Interactions and Nurturing Younger Researchers in Ocean Engineering”.

APPENDIX A : Raw data for two-compartment damage condition with ϕ_a = 20 deg, T_ϕ= 2.5 s. Single-phase simulations.

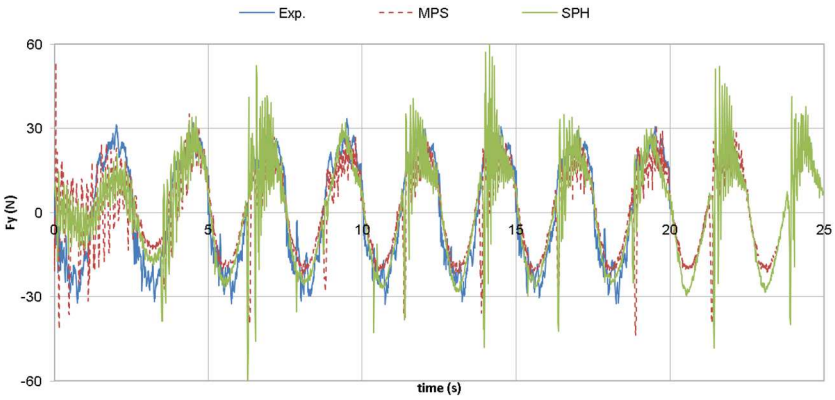

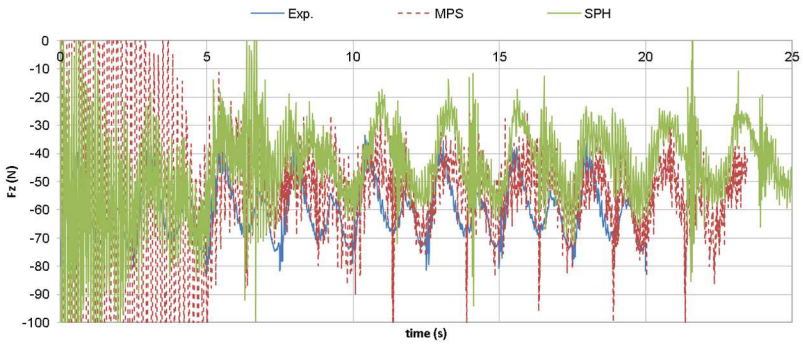

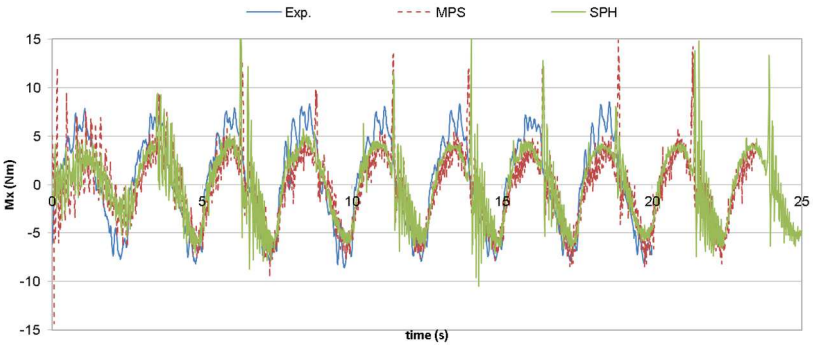

Fig A1: Comparison of raw hydrodynamic forces and moment for two-compartment damage condition with ϕ_a = 20 deg, T_ϕ = 2.5 s. Numerical results are for single-phase simulations.

We can notice that raw data is close to filtered data (see Fig. 10) for late periods after transient stage. We remind that data is averaged over the six last periods for computations and eight last for experiments. Besides, it can be noted that acoustic components are present in the weakly-compressible SPH raw data as expected. One of the effects of the averaging is to filter out these components, which is legitimate since filtering out this acoustic part permits theoretically to recover the incompressible solution.

REFERENCES

[1] Bačkalov I, Bulian G, Cichowicz J, Eliopoulou E, Konovessis D, Leguen J-F, Rosén A, Themelis N, Ship stability, dynamics and safety: Status and perspectives from a review of recent STAB conferences and ISSW events, Ocean Engineering, 2016, 116:312-349.

[2] Acanfora M, De Luca F, An Experimental Investigation on the Dynamic Response of a Damaged Ship with a realistic arrangement of the flooded compartment, Applied Ocean Research, 2017, 69:191-204.

[3] Siddiqui MA, Greco M, Lugni C, Faltinsen OM, Experimental studies of a damaged ship section in forced heave motion, Applied Ocean Research, 2019, 88:254-274.

[4] Gao Z, Gao Q, Vassalos D, Numerical study of damaged ship flooding in beam seas, Ocean Engineering, 2013, 61:77-87.

[5] Sadat-Hosseini H, Kim D-H, Carrica PM, Rhee SH, Stern F, URANS simulations for a flooded ship in calm water and regular beam waves, Ocean Engineering, 2016, 120:318-330.

[6] Gao Z, Wang Y, Su Y, On damaged ship motion and capsizing in beam waves due to sudden water ingress using the RANS method, Applied Ocean Research, 2020, 95:102047.

[7] Braidotti L, Degan G, Bertagna S, Bucci V, Marinò A, A Comparison of Different Linearized

Formulations for Progressive Flooding Simulations in Full-Scale, Procedia Computer Science, 2021,180:219-228.

[8] González V, Talens M, Riola JM, Valle J, Quesada T, Espín M, Numerical prediction of the dynamic behavior of a ro-ro ship after a hull side damage, Proceedings of the 8th International Conference on the Stability of Ships and Ocean Vehicles, 2003, 215-227, Madrid.

[9] Skaar D, Vassalos D, Jasionowski A, The use of a meshless CFD method in modelling progressive flooding and damaged stability of ships, Proceedings of the 9th International Conference on the Stability of Ships and Ocean Vehicles, 2006, 625-632, Rio de Janeiro.

[10] Le Touzé D, Marsh A, Oger G, Guilcher P-M, Khaddaj-Mallat C, Alessandrini B, Ferrant P, SPH simulation of green water and ship flooding scenarios, Journal of Hydrodynamics, 2010, 22(5):231-236.

[11] Oger G, Le Touzé D, Guilcher P-M, De Leffe M, Advances in SPH for naval hydrodynamics, Proceedings of the 30th Symposium on Naval Hydrodynamics, 2014, Hobart.

[12] Zhang A, Cao X, Ming F, Zhang Z, Investigation on a damaged ship model sinking into water based on three dimensional SPH method, Applied Ocean Research, 2013, 42:24-31.

[13] Guo K, Sun P-N, Cao X-Y, Huang X, A 3-D SPH model for simulating water flooding of a damaged floating structure, Journal of Hydrodynamics, 2017, 29(5):831-844.

[14] Ming F, Zhang AM, Cheng H, Sun PN, Numerical simulation of a damaged ship cabin flooding in transversal waves with Smoothed Particle Hydrodynamics method, Ocean Engineering, 2018, 165:336-352.

[15] Cao XY, Ming FR, Zhang AM, Tao L, Multi-phase SPH modelling of air effect on the dynamic flooding of a damaged cabin, 2018, Computers & Fluids, 163:7-19.

[16] Hashimoto H, Kawamura K, Sueyoshi M, Numerical simulation method for damaged ships under flooding condition, Proceedings of the 32nd International Conference on Ocean, Offshore and Arctic Engineering, 2014, Nantes.

[17] Hashimoto H, Kawamura K, Sueyoshi M, A numerical simulation method for transient behavior

of damaged ships associated with flooding, Ocean Engineering, 2017, 143:282-294.

[18] Hashimoto H, Kawakami N, Sueyoshi M. Numerical simulation method for coupling motions of a ship and tank fluid, Proceedings of the 11th International Conference on the Stability of Ships and Ocean Vehicles, 2012, 477–486, Athens.

[19] Cercos-Pita JL, Bulian G, Pérez-Rojas L, Francescutto A, Coupled simulation of nonlinear ship motions and a free surface tank, Ocean Engineering, 2015, 120:281-288.

[20] Zhang G, Wu J, Sun Z, El Moctar O, Zong Z, Numerically simulated flooding of a freely-floating two-dimensional damaged ship section using an improved MPS method, Applied Ocean Research, 2020, 101:102207.

[21] Souto-Iglesias A, Maciá, González LM, Cercos-Pita JL, On the consistency of MPS, Computer Physics Communication, 2013, 184:732-745.

[22] Souto-Iglesias, A., Macià, F., González, L.M., Cercos-Pita, J.L. Erratum: On the consistency of MPS (Computer Physics Communications (2013) 184:3 (732-745)), Computer Physics Communications, 2014, 185(2):595-598

[23] Abdelrazek AM, Kimura I, Shimizu Y, Comparison between SPH and MPS Methods for Numerical Simulations of Free Surface Flow Problems, Journal of Japan Society of Civil Engineers, Ser. B1 (Hydraulic Engineering), 2014, 70(4):67-72.

[24] Bakti FP, Kim KS, Kim MH, Park JC, Comparative Study of Standard WC-SPH and MPs solvers for Free Surface Academic Problems, International Journal of Offshore and Polar Engineering, 2016, 26(3):235-243.

[25] Amaro RA, Cheng LY, Buruchenko SK, A Comparison Between Weakly-Compressible Smoothed Particle Hydrodynamics (WCSPH) and Moving Particle Semi-Implicit (MPS) Methods for 3D Dam-Break Flows, International Journal of Computational Methods, 2021, 18(2):2050036.

[26] Khayyer A, Gotoh H, Falahaty H, Shimizu Y, An enhanced ISPH–SPH coupled method for simulation of incompressible fluid–elastic structure interactions, Computer Physics Communications, 2018, 232:139-164.

[27] Khayyer A, Shimizu Y, Gotoh H, Hattori S, Multi-resolution ISPH-SPH for accurate and efficient simulation of hydroelastic fluid-structure interactions in ocean engineering, Ocean Engineering, 2021, 226:108652.

[28] Gao Z, Wang Y, Su Y, Chen L, Numerical study of damaged ship's compartment sinking with air compression effect, Ocean Engineering, 2018, 147,:8-76.

[29] Khayyer A, Gotoh H, A Multiphase Compressible–Incompressible Particle Method for Water Slamming, International Journal of Offshore and Polar Engineering, 2016, 26(1):20-25.

[30] Koshizuka S, Oka Y. Moving particle semi-implicit method for fragmentation of incompressible fluid, Nuclear Science and Engineering, 1996, 124:421-434.

[31] Sueyoshi M, Kashiwagi M., Naito S. Numerical simulation of wave-induced nonlinear motions of a two-dimensional floating body by the moving particle semi-implicit method, Journal of Marine Science and Technology, 2008, 13:85-94.

[32] Sueyoshi M. Numerical Simulation of Tank Sloshing with Thin Plate Structures by Using a Particle Method, Proceedings of the 19th International Offshore and Polar Engineering Conference, 2009, 3:303-307, Osaka.

[33] Ikeda H., Koshizuka S., Oka Y., Park H.S., Sugimoto J. Numerical Analysis of Jet Injection Behavior for Fuel-Coolant Interaction using Particle Method, Journal of Nuclear Science and Technology, 2001, 38(3):174-182.

[34] Tanaka M, Masunaga T. Stabilization and smoothing of pressure in MPS method by Quasi-Compressibility, Journal of Computational Physics, 2010, 229:4279–4290.

[35] Gotoh H., Khayyer A., On the state-of-the-art of particle methods for coastal and ocean engineering, Coastal Engineering Journal, 2018, 60 (1):79-103.

[36] Lucy L.B. A numerical approach to the testing of the fission hypothesis, Astronomical Journal, 1977, 82:1013-24.

[37] Gingold R.A., Monaghan J.J. Smoothed particle hydrodynamics: theory and application to non-spherical stars, Mon. Not. R. Astron. Soc., 1977, 181:375-89.

[38] Monaghan J.J. Simulating free surface flows with SPH, 1994, Journal of Computational Physics, 110:399-406.

[39] Marrone S., Colagrossi A., Di Mascio A., Le Touzé D., Prediction of energy losses in water impacts using incompressible and weakly compressible models, 2015, Journal of Fluids and Structures, 54:802-822.

[40] Wendland H. Piecewise polynomial, positive definite and compactly supported radial functions of minimal degree, Advances in Computational Mathematics, 1995, 4:389-396.

[41] Monaghan J.J. Smoothed Particle Hydrodynamics, 2005, Reports on Progress in Physics, 68:1703-1759.

[42] Vila J.-P. On Particle Weighted Methods and Smooth Particle Hydrodynamics, Mathematical Models and Methods in Applied Science, 1999, 9(2):161-209.

[43] Oger G., Marrone S., Le Touzé D., De Leffe M., SPH accuracy improvement through the combination of a quasi-Lagrangian shifting transport velocity and consistent ALE formalisms, Journal of Computational Physics, 2016, 313:76-98.

[44] Chiron L., De Leffe M., Oger G., Le Touzé D., Fast and accurate SPH modelling of 3D complex wall boundaries in viscous and non viscous flows, Computer Physics Communications, 2019, 294:93-111.

[45] Oger G., Le Touzé D., Guibert D., De Leffe M., Biddiscombe J., Soumagne J., Piccinali J.-G., On distributed memory MPI-based parallelization of SPH codes in massive HPC context, Computer Physics Communications, 2016, 200:1-14.

[46] Colagrossi A., Antuono M., Le Touzé D., Theoretical considerations on the free-surface role in the smoothed-particle-hydrodynamics model, Physical Review E, 2009, 79: 056701.

[47] Hammani I., Marrone S., Colagrossi A., Oger G., Le Touzé D., Detailed study on the extension of the δ-SPH model to multi-phase flow, Computer Methods in Applied Mechanics and Engineering, 2020, 368:113189.

[48] Grenier N., Antuono M., Colagrossi A., Le Touzé D., Alessandrini B., An Hamiltonian SPH

formulation for Interfacial and Free-Surface Flows using a Shepard Kernel, Journal of Computational Physics, 2009, 228:8380–8393.

[49] Marrone S., Colagrossi A., Di Mascio A., Le Touzé A., Analysis of free-surface flows through energy considerations: Single-phase versus two-phase modeling, 2016, Physical Review E, 93(5):0505113.